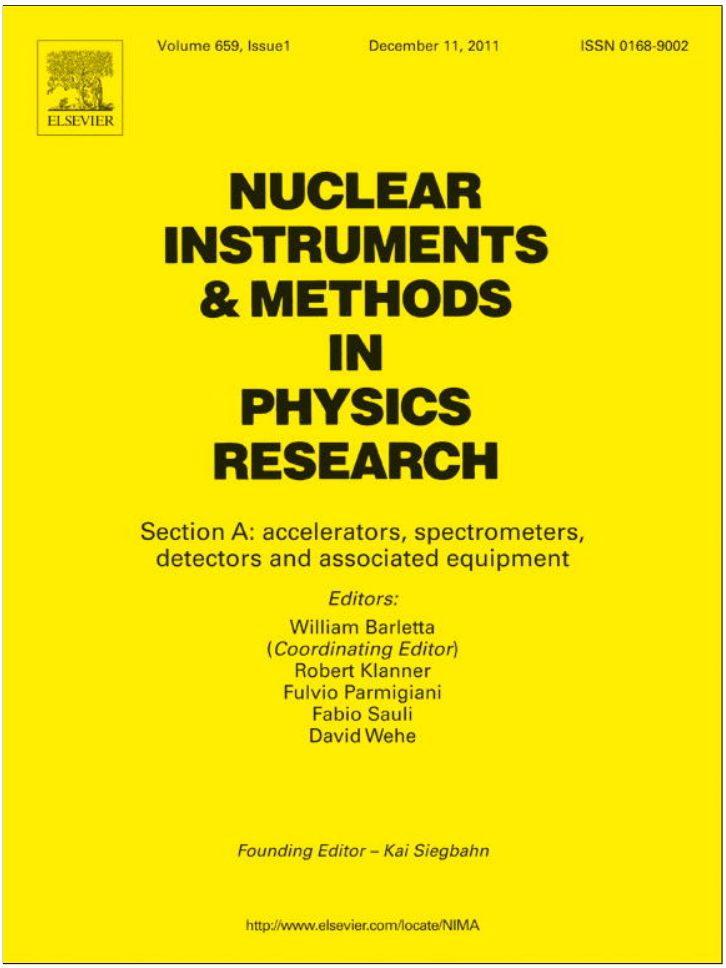

Nuclear Instruments and Methods in Physics Research A 659 (2011) 21–29

Contents lists available at SciVerse ScienceDirect

Nuclear Instruments and Methods in Physics Research A

journal homepage: www.elsevier.com/locate/nima

The beam energy measurement system for the Beijing electron–positron collider

E.V. Abakumova [a], M.N. Achasov [a,*], V.E. Blinov [a], X. Cai [b], H.Y. Dong [b], C.D. Fu [b], F.A. Harris [c], V.V. Kaminsky [a], A.A. Krasnov [a], Q. Liu [c], X.H. Mo [b], N.Yu. Muchnoi [a], I.B. Nikolaev [a], Q. Qin [b], H.M. Qu [b], S.L. Olsen [c], E.E. Pyata [a], A.G. Shamov [a], C.P. Shen [c], K.Yu. Todyshev [a], G.S. Varner [c], Y.F. Wang [b], Q. Xiao [b], J.Q. Xu [b], J.Y. Zhang [b], T.B. Zhang [b], Y.H. Zhang [b], A.A. Zhukov [a]

[a] Budker Institute of Nuclear Physics, Siberian Branch of the Russian Academy of Sciences, 11 Lavrentyev, Novosibirsk 630090, Russia
[b] Institute of High Energy Physics, Beijing 100049, People's Republic of China
[c] University of Hawaii, Honolulu, Hawaii 96822, USA

ARTICLE INFO

Article history:
Received 24 August 2011
Accepted 25 August 2011
Available online 3 September 2011

Keywords:
Compton backscattering
Beam energy calibration
Collider BEPC-II
τ-charm factory

ABSTRACT

The beam energy measurement system (BEMS) for the upgraded Beijing electron–positron collider BEPC-II is described. The system is based on measuring the energies of Compton back-scattered photons. The relative systematic uncertainty of the electron and positron beam energy determination is estimated as 2×10^{-5}. The relative uncertainty of the beam's energy spread is about 6%.

1. Introduction

The upgraded Beijing electron–positron collider (BEPC-II) is a τ-charm factory with a center of mass energy range from 2.0 to 4.6 GeV and a design peak luminosity of $10^{33}\,\mathrm{cm}^{-2}\,\mathrm{s}^{-1}$ [1]. For experiments at BEPC-II, the BESIII (Beijing spectrometer) detector with high efficiency and resolution both for charged and neutral particles was constructed [2]. BESIII started data taking in 2008. The BESIII research program covers charmonium physics, D-meson physics, spectroscopy of light hadrons and τ-lepton physics [3]. The τ-lepton is a fundamental particle, and its mass is a Standard Model parameter, which requires that its mass be determined with high precision. The measurements of the ψ and D meson masses are also of interest.

The current value of the τ mass, m_τ, is 1776.82 ± 0.16 [4]. In BEPC-II/BESIII, the mass will be measured using the threshold scan method. The accuracy of the measurement was studied in Refs. [5,6]. Two weeks of data taking will lead to a statistical uncertainty of less then 50 keV. The systematic uncertainty (without the accuracy of beam energy determination) is about 20 keV and includes uncertainties of the luminosity, detection efficiency, branching fraction, background, energy spread, and theoretical uncertainty. The most important source of uncertainty is the accuracy of the absolute beam energy determination.

In some cases, the energy scale of colliders can be calibrated with extremely high accuracy using the resonant depolarization technique [7]. But this approach is not applicable for e^+e^- factories, where the great advance in luminosity is made possible by fast bunch-to-bunch feedback systems that usually have a strong depolarization impact on the beam. There are two possible methods of the beam energy determination at BEPC-II. First is a calibration of the energy scale from scan of the J/ψ and ψ' resonances [8]. The expected accuracy in this case is about 100 keV.

Another possibility is the beam energy measurement using Compton back-scattering of monochromatic laser radiation on the $e^\pm$ beams. This approach was developed and experimentally proved in Refs. [9–12]. At the BESSY-I and BESSY-II storage rings, the relative accuracies of energy measurement of about 10^{-4} and 3×10^{-5} for the beam energies of 800 and 1700 MeV, respectively, were achieved [11]. In collider experiments, this method was applied at VEPP-4M [12]. Based on the VEPP-4M experience, such a system was proposed and constructed for BEPC-II [13,14]. In this paper, the system design and performance are reported.

2. The Compton back-scattering approach

Let us consider the Compton scattering process in a case where the angle α between initial particles is equal to π and their

* Corresponding author.
E-mail address: achasov@inp.nsk.su (M.N. Achasov).

0168-9002/$ - see front matter © 2011 Elsevier B.V. All rights reserved.
doi:10.1016/j.nima.2011.08.050

energies are $\omega_0 \ll m_e \ll \varepsilon$ (Fig. 1). Here ω_0 and ε are the energies of the initial photon and electron, respectively. The back-scattered photons with $\theta = 0$ have the maximal energy (Fig. 2), and the energy spectrum of the scattered photons has a sharp edge at the maximal energy (Fig. 3).

The general idea is based on the following:

- The maximal energy of the scattered photon ω_{max} is related with the electron energy ε by the kinematics of Compton scattering [13]:

$$\omega_{max} = \frac{\varepsilon^2}{\varepsilon + m_e^2/4\omega_0} \tag{1}$$

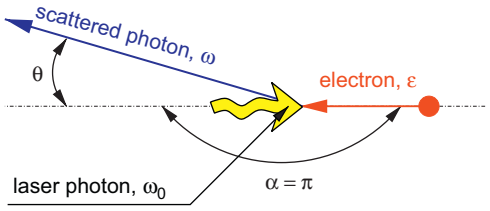

Fig. 1. The Compton scattering process. ε, ω_0, and ω are the particles energies, and $\alpha = \pi$.

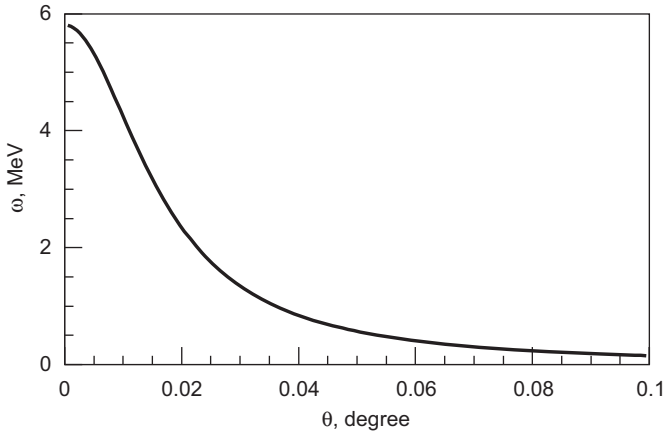

Fig. 2. The dependence of the scattered photon energy ω on the angle θ between the initial electron and the final photon in the Compton scattering process. The initial electron and photon energies are $\omega_0 = 0.12$ eV and $\varepsilon = 1770$ MeV, respectively, and $\alpha = \pi$.

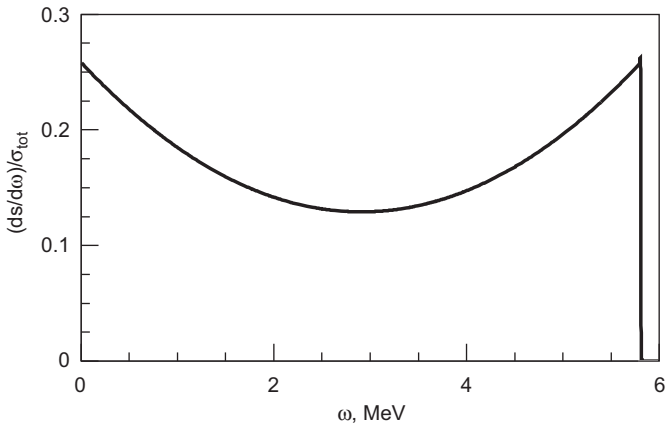

Fig. 3. Energy spectrum of scattered Compton photons. The initial electron and photon energies are $\omega_0 = 0.12$ eV and $\varepsilon = 1770$ MeV, respectively, and $\alpha = \pi$.

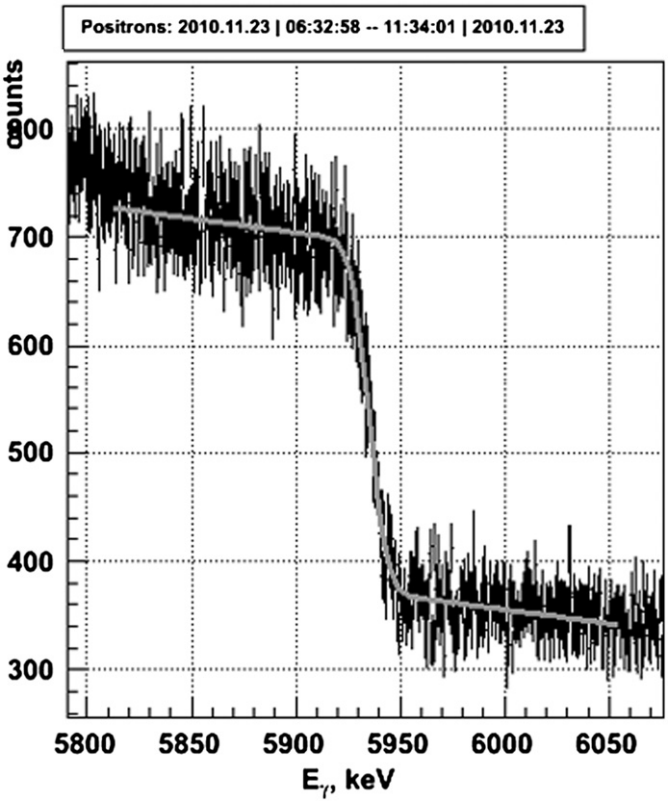

Fig. 4. The measured edge of the scattered photons energy spectrum. The line is the fit result.

If one measures ω_{max}, then the electron energy can be calculated:

$$\varepsilon = \frac{\omega_{max}}{2}\left[1 + \sqrt{1 + \frac{m_e^2}{\omega_0 \omega_{max}}}\right]. \tag{2}$$

- The ultra-high energy resolution ($\sim 10^{-3}$) of commercially available High Purity Germanium (HPGe) detectors allows the statistical accuracy in the beam energy measurement to be at the level of $\delta\varepsilon/\varepsilon \simeq 10^{-5}$.
- The systematical accuracy is mostly defined by absolute calibration of the detector energy scale. Accurate calibration can be performed in the photon energy range up to about 10 MeV by using γ-active radionuclides.

The measurement procedure is as follows. As a source of initial photons, the monochromatic laser radiation with $\omega_0 \approx 0.12$ eV is used. The laser light is put in collision with the electron or positron beams, and the energy of the back-scattered photons is precisely measured using the HPGe detector. The maximal energy of the scattered photons is determined by fitting the abrupt edge in the energy spectrum by the erfc-like function (Fig. 4). The relation between the measured ω_{max} and the beam energy ε is shown in Fig. 5. The detector energy scale is accurately calibrated by using well-known radiative sources of γ-radiation (Fig. 5).

3. The beam energy measurement system for BEPC-II

The beam energy measurement system is located at the north beam crossing point of the BEPC-II storage rings (Fig. 6). This location allows measurement of the electron and positron beams

energy by the same HPGe detector. The layout schematic of the system is shown in Fig. 7.

The system consists of the laser source, optical and laser-to-vacuum insertion systems to transport the laser beam into the interaction regions where the laser beam collides with either the electron or positron beam, and the HPGe detector to measure back-scattered photons. The laser and optical system elements are deployed in the corridor outside the collider hall.

The laser and electron (positron) beams interact in the straight sections of the collider's rings beyond the R2IAMB (R1IAMB) dipole magnets. The total yield of scattered photons was estimated in Ref. [13] and is about 17 000 gammas per second, per 1 mA of electron (positron) beam current, per 1 W of laser power.

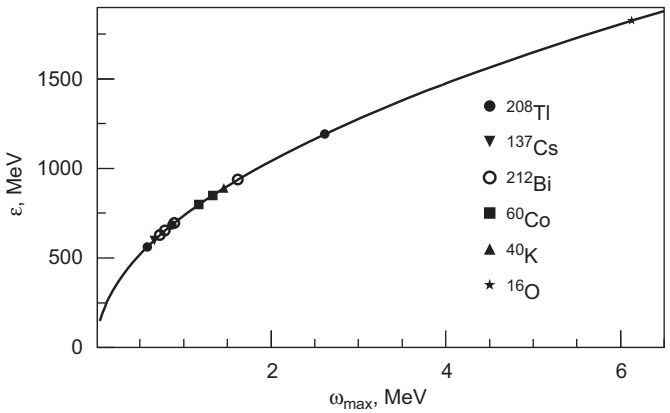

Fig. 5. Relation between ω_{max} and ε (solid line). Dots are the energies of γ-active radionuclide reference lines for the HPGe detector calibration. The initial photon energy is $\omega_0 = 0.12$ eV.

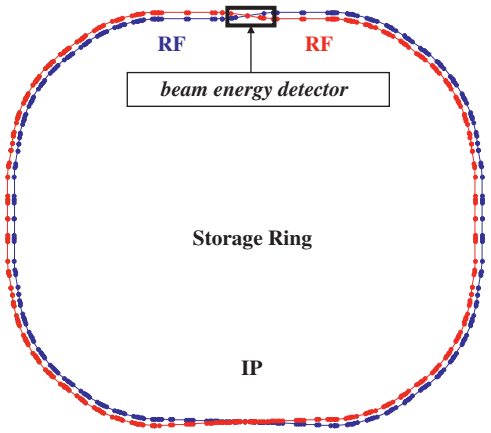

Fig. 6. Location of the energy measurement system at the BEPC-II collider. The deployment place is indicated as "beam energy detector".

3.1. Laser and optical system

The source of initial photons is the GEM Selected 50^{TM} CO_2 laser from Coherent, Inc.. It is a continuous operation (CW), high power, and single-line laser. It provides 25 W of CW power at the wavelength $\lambda_0 = 10.835231$ μm (γ-quantum energy $\omega_0 = 0.114426901$ eV), which corresponds to the 10P42 transition in the carbon dioxide molecule [15]. ω_0 is known with relative accuracy better then 0.1 ppm. The relative width of the laser photon spectrum is $\sigma_\omega/\omega_0 \approx$ 3 ppm. This wavelength was adopted in order to avoid any interference between γ-radiation lines of radiative sources, used for HPGe detector calibration, and the Compton edges of all interesting energy points in the τ-charm energy region (Fig. 8). The laser is installed on a special support which can be adjusted as necessary.

The optical system includes the following units which are situated along the collider wall (Fig. 7):

1. Two ZnSe lenses with focal lengths of $f = 40$ cm. The laser beam is focused at the BEPC-II vacuum chamber entrance flange, where the geometrical aperture is minimal: vertical size $\times$ horizontal size is 14 mm $\times$ 50 mm. The total distance from the laser output aperture to the entrance flange of the BEPC-II vacuum chamber is about 18 m. The lenses are placed at 300 and 382 cm from the laser and provide the laser beam transverse size at the flange from 0.20 to 0.25 cm.

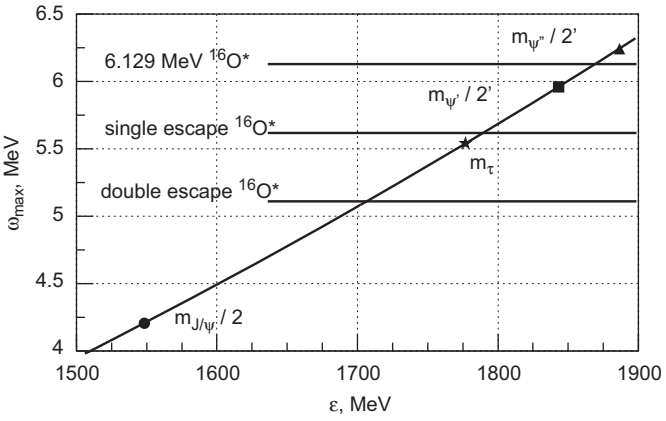

Fig. 8. The relation between beam energy ε and energy of back-scattered Compton photons ω_{max}. The γ lines of $^{16}O^*$ are also shown.

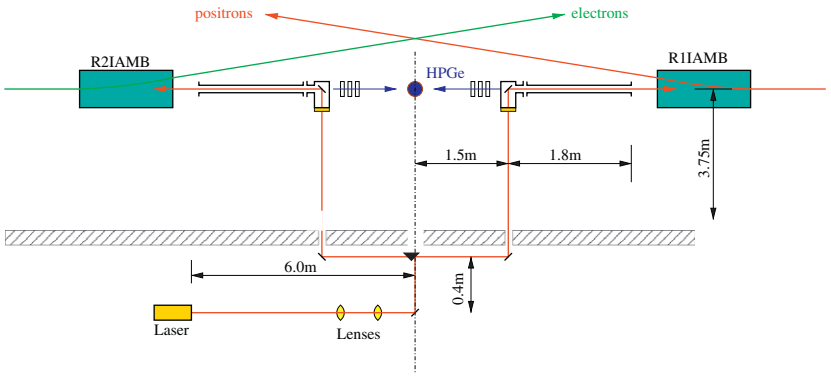

Fig. 7. Simplified schematic of the energy measurement system. The positron and electron beams are indicated. R1IAMB and R2IAMB are accelerator magnets, and the HPGe detector is represented by the dot at the center. The shielding wall of the beam tunnel is shown cross-hatched, and the laser is located outside the tunnel.

2. A 45° mirror, which reflects the beam through an angle of 90° towards the movable prism.
3. A movable reflector prism which directs the laser beam towards the right or left mirror.
4. Two mirrors to reflect the right or left-traveling laser beam into the collider tunnel through holes in the concrete wall. The laser beam is incident on a viewport in a vacuum pipe extension of the beam pipe. The mirrors are installed on special supports that allow precise vertical and horizontal angular alignment by the use of stepping motors (one step equals 1.5×10^{-6} rad).

3.2. Laser-to-vacuum insertion system

The insertion of the laser beam into the vacuum chamber is performed using the laser-to-vacuum insertion system. The system is the special stainless steel vacuum chamber with a GaAs entrance viewport [16] and water cooled copper mirror (Fig. 9). In the vacuum chamber, the laser beam is reflected through an angle of 90° by the copper mirror. After back-scattering, the photons return to the mirror, pass through it, leave the vacuum chamber, and are detected by the HPGe detector. Note, the copper mirror protects the view port against high power synchrotron radiation due to low reflectivity of high energy photons (less than 1%) from a metallic surface.

The copper mirror design is shown in Fig. 10. The mirror can be turned by bending the vacuum flexible bellows, so the angle between the mirror and the laser can be adjusted as necessary. Synchrotron radiation (SR) photons heat the mirror. In order to reduce the heating of the mirror, it is placed 1.8 m from the BEPC-II vacuum chamber flange. The SR power absorbed by the mirror is about 200 W. The extraction of heat is provided by a water cooling system. To prevent adsorption of residual gas molecules on the mirror surface, it is covered with a 0.5 μm thick gold layer.

The viewport based on the GaAs mono-crystal provides:

1. transmission spectrum from 0.9 up to 18 μm,
2. baking out of the vacuum system up to 250 °C,
3. extra high vacuum.

The viewport design is shown in Fig. 11. It includes a 304 L steel DN63 conflat flange and a GaAs crystal plate with diameter of 50.8 mm and thickness of 3 mm. In order to compensate mechanically for the difference of the GaAs and stainless steel thermal expansion coefficients, the GaAs plate is brazed with pure soft lead to a titanium ring, which in turn is brazed with AgCu alloy to the stainless steel ring. The stainless steel ring is welded to the flange. To avoid decomposition of the GaAs plate during brazing, it is covered with a 0.6 μm thick SiO_2 film using gas-phase deposition. The transmission spectra of the plate before and after covering are shown in Fig. 12. The transmission of the plate increases from 55% to 60 % at the CO_2 laser wavelength $\lambda = 10.6$ μm and from 20% to 35% at $\lambda = 1$ μm.

After installation at BEPC-II, the vacuum chambers were baked out at 250 °C for 24 h. A pressure of 2×10^{-10} Torr was obtained. The residual gas spectrum is shown in Fig. 13.

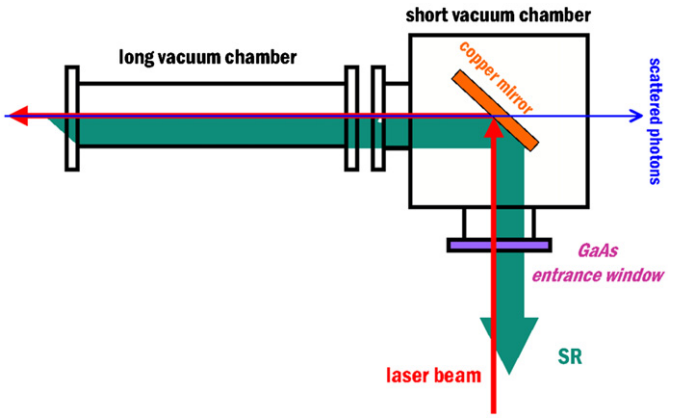

Fig. 9. Simplified schematic of the laser-to-vacuum insertion assembly.

3.3. Adjustment of the optical elements

The optical elements of the system were adjusted using SR. The copper mirrors of the vacuum chambers and the mirrors of the optical system were adjusted in such a way, that the SR light comes to the laser output window. Actually the GaAs is not transparent for visible light (Fig. 12) but transmits infrared radiation. In order to detect the infrared light, IR-sensitive video cameras were used.

3.4. HPGe detector

The purpose of a HPGe detector is to convert γ-rays into electrical impulses which can be used with suitable signal processing, to determine their energy and intensity. A HPGe detector is a large germanium diode of the p-i-n type operated in the reverse bias mode. At a suitable operating temperature (normally $\simeq 100$ K), the barrier created at the junction reduces the leakage current to acceptably low values. Thus an electric field can be applied that is sufficient to collect the charge carriers liberated by the ionizing radiation.

For the BEPC-II energy calibration system, we use the coaxial HPGe detector manufactured by ORTEC (model GEM25P4-70).

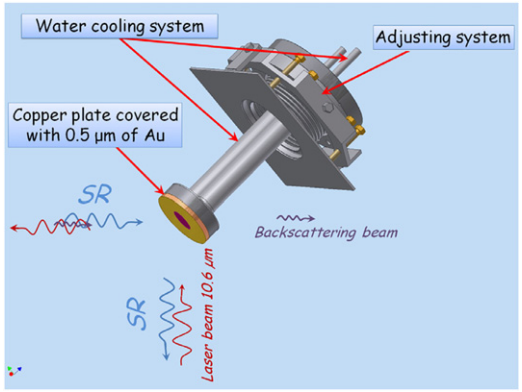

Fig. 10. Copper mirror.

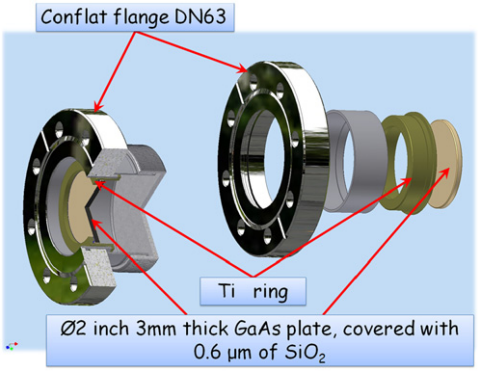

Fig. 11. The GaAs viewport.

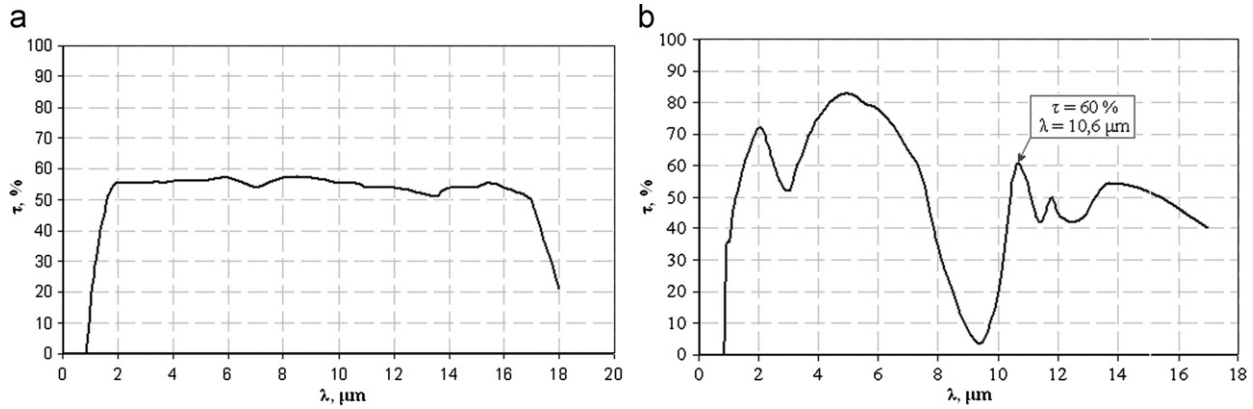

Fig. 12. The transmission spectra of GaAs are shown for (a) the 3 mm thick original plate; (b) the plate covered by SiO2 film with thickness of 0.6 μm.

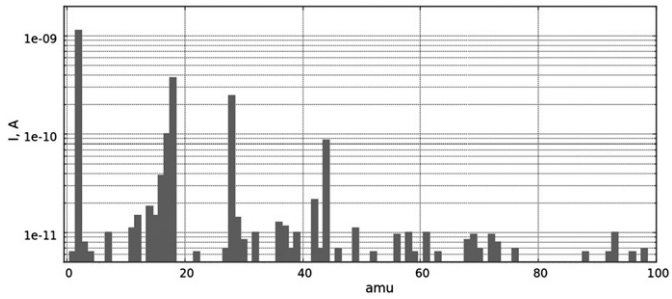

Fig. 13. Residual gas spectrum.

It has diameter of 57.8 mm and height of 52.7 mm with 31.2% relative efficiency.[1] The energy resolution for the 1.33 MeV line of ^{60}Co is 1.74 keV (FWHM). The detector is connected to the multi-channel analyzer ORTEC DSpec Pro (MCA), which transfers data using the USB port of the computer.

The HPGe spectrum has $2^{14}=16\,384$ channels. The bin error for each channel is defined as

$$\Delta N=\sqrt{N+(\zeta N)^2} \tag{3}$$

where N is number of counts in the channel and ζ corresponds to the MCA differential non-linearity, which is $\zeta=0.02$ according to the MCA specifications.

Since the HPGe detector is located near the collider's beam pipes, background due to beam loss is extremely high. In order to protect the HPGe detector from background, it is surrounded by 5 cm of lead on the sides, by 1.5 cm of iron below, and by 5 cm of lead above. The detector is also shielded by 10 cm of paraffin on all sides. Since the main background comes from the beam direction, an additional 11 cm of lead is installed in these directions. Another 10 cm of lead can be moved into the beam using movable stages to shield from the beam direction that is not being measured and moved out when the beam is being measured.

4. Data acquisition system

The BEMS data acquisition system is shown in Fig. 14. The MCA digitizes the signal from the HPGe detector and produces the energy spectrum. It is connected to a Windows PC. All spectra processing, monitoring, and control over the devices involved in the BEMS is concentrated in another PC, under the control of Linux.

The data acquisition procedure is as follows. The HPGe detector measurements are read every few seconds, and the detector counting rate is calculated. If the requested acquisition time has elapsed, or if conditions of the spectrum acquisition changed sufficiently, the current spectrum is saved to a file and the next spectrum acquisition cycle is launched. Simultaneously, another process periodically requests information from the BEPC-II database and writes the BEPC-II parameters, such as beam currents, lifetimes, and luminosity, to the file.

After finishing the spectrum acquisition cycle, another program processes the spectrum; it calibrates the energy scale, finds the Compton edge, and calculates the beam energy. The beam energy is written into the BEPC-II database. Since the BEPC-II parameters and the detector counting rate are saved during the spectra acquisition, conditions of any acquired spectrum can be analyzed at any time.

During data taking, mirrors are adjusted automatically to provide maximal photon/electron (positron) interaction efficiency, using the feedback from the detector counting rate. The prism directing the laser beam to either the electron or positron beams is controlled by the same program, as are the movable stages that move the extra lead protection in and out of the beam. The processing of the beam energy measurement is fully automated by a script controlling the mirrors, the prism, and the movable shielding.

5. Data processing

The processing of the spectrum (Fig. 15) includes calibration of the energy scale, Compton edge fitting and the calculation of the beam energy.

The energy scale must be calibrated in the range from 2 to 8 MeV. This is the energy range of back-scattered photons at BEPCII with beam energies from 1000 to 2100 MeV (Fig. 5). The following sources were used in this work:

- ^{137}Cs: $E_\gamma=661.657\pm0.003$ keV
- ^{60}Co: $E_\gamma=1173.228\pm0.003$ keV
- ^{60}Co: $E_\gamma=1332.492\pm0.004$ keV
- ^{16}O*: $E_\gamma=6129.266\pm0.054$ keV[2]

[1] The efficiency of each detector is usually specified by a parameter called *relative detection efficiency*. The *relative detection efficiency* of coaxial germanium detectors is defined at 1.33 MeV relative to that of a standard 3 in. diameter, 3 in. long *NaI*(*Tl*) scintillator.

[2] The [^{238}Pu ^{13}C] γ source is used. The nuclear reaction occurs in this source: $\alpha+^{13}C\rightarrow n+^{16}O^*$. The excited oxygen emits γ-rays with energy of 6129.266 ± 0.054 keV. [17]

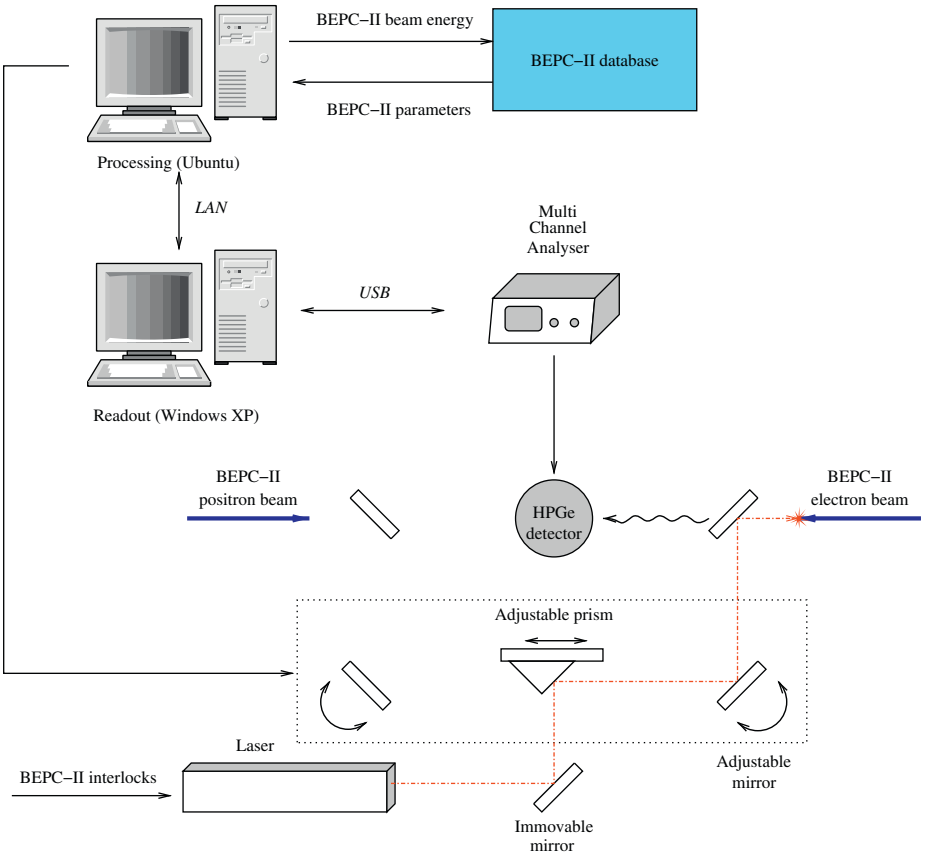

Fig. 14. Layout of data acquisition system.

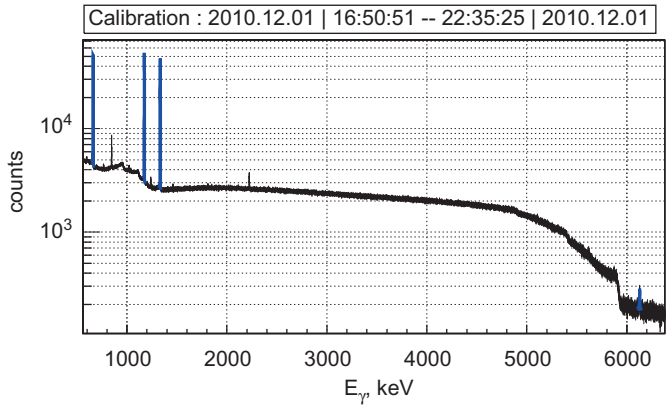

Fig. 15. The energy spectrum detected by the HPGe detector is shown. Several peaks, corresponding to monochromatic γ-radiation radiative sources, as well as the abrupt edge of the Compton photons spectrum slightly below 6000 keV are clearly seen.

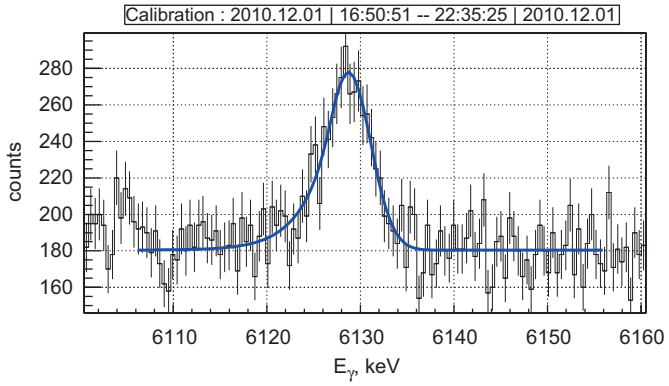

Fig. 16. The fit to the $^{16}O^*$ 6.13 MeV peak. $\chi^2/NDF = 87.2/105$.

The goal of HPGe detector calibration is to obtain the coefficients needed for conversion of the HPGe detector's ADC counts into corresponding energy deposition, measured in units of keV, as well as the determination of the detector's response function parameters. The following response function is used:

$$f(x,x_0,\sigma,\xi)=\frac{N}{\sqrt{2\pi}}\sigma\cdot\begin{cases}\exp\left\{-\frac{(x-x_0)^2}{2\sigma^2}\right\}, & x>x_0-\xi\cdot\sigma\\ \exp\left\{\frac{\xi^2}{2}+\frac{\xi(x-x_0)}{\sigma}\right\}, & x\le x_0-\xi\cdot\sigma\end{cases} \quad (4)$$

$$\frac{1}{N}=\int_{-\infty}^{+\infty}f(x,x_0,\sigma,\xi)dx=\frac{1}{2}\,\mathrm{erfc}\left(-\frac{\xi}{\sqrt{2}}\right)+\frac{1}{\sqrt{2\pi}}\xi\exp\left(-\frac{\xi^2}{2}\right). \quad (5)$$

Here x_0 is the position of the maximum, ξ is an asymmetry parameter, and σ is the full-width of the Gaussian distribution at half-maximum divided by 2.36.

The calibration procedure is as follows:

1. Peak searching is performed using a ROOT algorithm based on Refs. [18–20];
2. The found peaks are identified using the atlas of the well known radiative lines;
3. The peaks which correspond to calibration lines are fitted by the sum of signal and background distributions, $f(x,x_0,\sigma,\xi)+p_1(x)$ (Fig. 16), where $p_1(x)$ is a first-order polynomial. The free

parameters of the fit are x_0, σ, ξ, and the coefficients of the polynomial.

4. Using the fit results, the energy dependencies of the response function (Eq. (4)) parameters are determined. The σ energy dependence (Fig. 17) is described by the formula:

$$\sigma_E = \sqrt{K_0 + FE_\gamma} \tag{6}$$

where E_γ is the photon energy, $K_0 = 0.772 \pm 0.020\ \text{keV}^2$, and $F = 0.56 \pm 0.02$ eV. The energy dependence of the asymmetry parameter ξ is approximated with an empirical function, $g(x) = p_0 + p_1 \exp(-p_2 x)$ (Fig. 18). In order to obtain the correction to the measured energy due to spectrometer scale nonlinearity, the difference between positions of the calibration peaks x_0 and their known reference values are fitted by a second-order polynomial (Fig. 19).

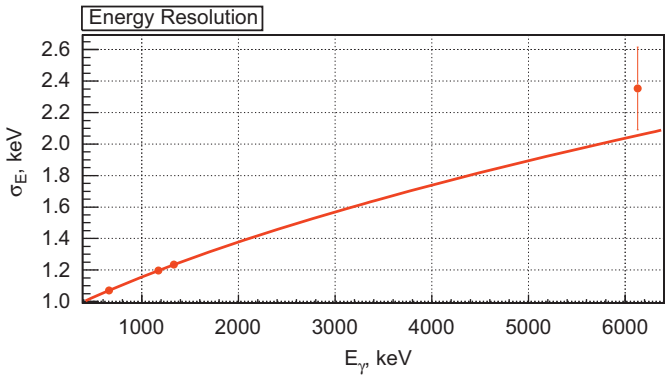

Fig. 17. σ_E vs the photon energy, fitted by Eq. (6). The fit results in $\chi^2/NDF = 1.3/2$.

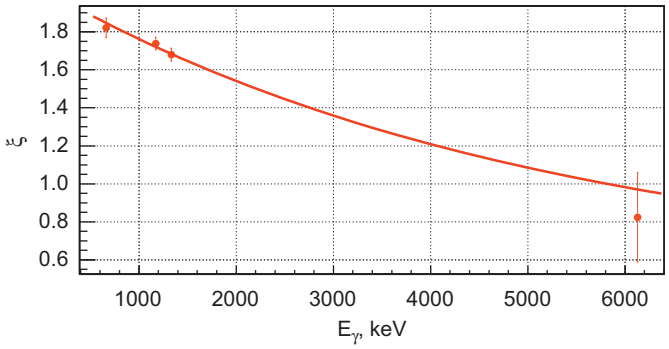

Fig. 18. Asymmetry parameter ξ vs photon energy.

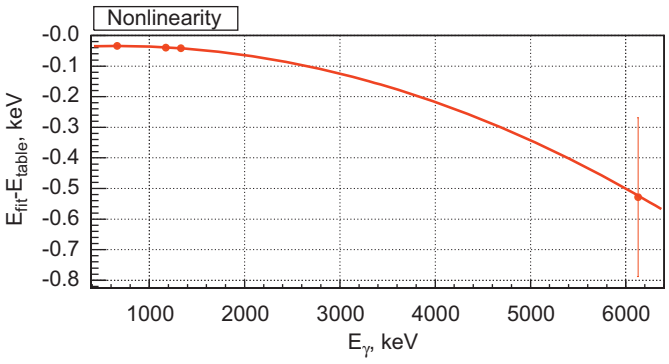

Fig. 19. Energy dependence of the differences between the calibration peaks from their true values.

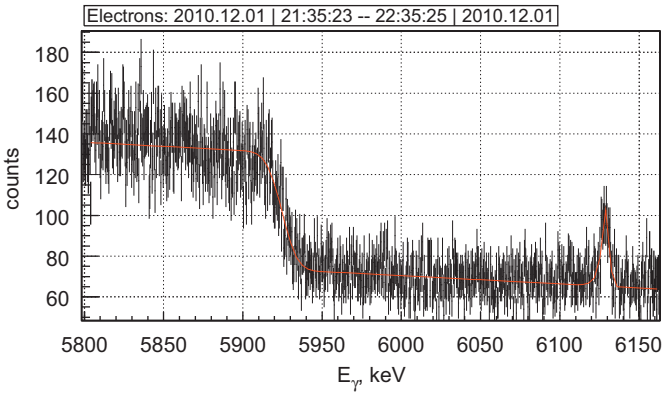

Fig. 20. The energy spectrum of back-scattered photons near ω_{max} and the fit function. The 6.129 MeV peak is also seen.

The edge of the back-scattered photon spectrum (Fig. 20) is fitted by the function:

$$S_2(x,x_0,\sigma,\sigma_s,\xi) = \int_x^{+\infty} S_1(y,x_0,\sigma,\sigma_s,\xi)\,dy + p_1(x). \tag{7}$$

Here $p_1(x)$ takes into account the background contribution, and S_1 is a convolution of the step function $\theta(x_0 - x)$:

$$\theta(x_0 - x) = \begin{cases} 0, & x < x_0 \\ 1, & x > x_0 \end{cases} \tag{8}$$

which describes the "pure" edge shape with the HPGe detector response function (Eq. (4)) and a Gaussian:

$$g(x,x_0,\sigma_s) = \frac{1}{\sqrt{2\pi}}\sigma_s \exp\left\{-\frac{(x-x_0)^2}{2\sigma_s^2}\right\} \tag{9}$$

which takes into account the energy spread of back-scattered photons due to energy distribution of the collider beam.

$$\begin{aligned} S_1(x,x_0,\sigma,\sigma_s,\xi) &= \frac{N}{2\sqrt{2\pi}} \\ &\times \left[\frac{1}{\sigma}\exp\left(\frac{\xi^2}{2}\left(1+\frac{\sigma_s^2}{\sigma^2}\right)+\frac{\xi x}{\sigma}\right)\cdot \operatorname{erfc}\left(\frac{\xi(\sigma^2+\sigma_s^2)+x\sigma}{\sqrt{2}}\sigma\sigma_s\right)\right. \\ &\left. + \frac{1}{\sqrt{\sigma^2+\sigma_s^2}}\exp\left(-\frac{x^2}{2(\sigma^2+\sigma_s^2)}\right)\cdot \operatorname{erfc}\left(-\frac{\xi(\sigma^2+\sigma_s^2)+x\sigma}{\sqrt{2(\sigma^2+\sigma_s^2)}}\sigma_s\right)\right]. \end{aligned} \tag{10}$$

The edge position $\omega_{max} \equiv x_0$, σ_s, and the coefficients of the first-order polynomial $p_1(x)$ are the free parameters of the fit. Using the ω_{max} value obtained from the fit, the average beam energy ε_{nip} (*nip* denotes north interaction region) in the e−γ interaction region is calculated according to formula (2). Taking into account the energy losses due to synchrotron radiation, the beam energy in the south interaction point (*sip*) is obtained as

$$\varepsilon_{sip}(\text{MeV}) = \varepsilon_{nip}(\text{MeV}) + 4.75 \times 10^{-3} * (0.001 \cdot \varepsilon_{nip}(\text{MeV}))^4. \tag{11}$$

6. System performance

The system was put in operation and tested with beams of energy about 1840 MeV. The relative statistical accuracy of the beam energy determination of about 5×10^{-5} was achieved after approximately 1 h of data taking. The systematical accuracy was studied by comparison of the well known mass of the ψ' resonance $m_{\psi'} = 3686.09 \pm 0.04$ MeV [4] with its value obtained using the BEMS.

In order to obtain the ψ' mass two scans of the resonance energy region were done with a total integrated luminosity of

about 3.95 pb^{-1}. The data were collected at 12 energy points over 36 h. The ψ' mass was measured as follows:

1. The multihadronic $e^+e^- \to hadrons$ events were selected.
2. The events of $e^+e^- \to \gamma\gamma$ were used to determine the integrated luminosity L:

$$L = \frac{N^{\gamma\gamma}}{\sigma^{\gamma\gamma}(w)}, \tag{12}$$

where $N^{\gamma\gamma}$ and $\sigma^{\gamma\gamma}$ are the selected number of events and cross-section obtained using Monte Carlo simulation, and w is the center of mass energy.

3. The resonance mass was obtained from the fit of the number of $e^+e^- \to hadrons$ events expected, $M^{mhad} = \sigma^{mhad}L$, to the number of detected multihadronic events N^{mhad}. Here σ^{mhad} is the expected cross-section of $e^+e^- \to hadrons$:

$$\sigma^{mhad}(w) = \sigma_{bg} \cdot \left(\frac{3686\ \text{MeV}}{w}\right)^2 + \varepsilon \cdot \sigma_{res}(w,m,\sigma_w) \tag{13}$$

where m is the ψ' meson mass, σ_{bg} is the nonresonant background cross-section, ε is the detection efficiency, σ_{res} is the cross-section of the ψ' resonance production $\sigma_0(w,m)$ [21] convoluted with the beam energy spread σ_w:

$$\sigma_{res}(w,m,\sigma_W) = \int_{-\infty}^{+\infty} \frac{\exp\left(-\frac{(w-w')^2}{2\sigma_w^2}\right)}{\sqrt{2\pi}} \sigma_w \sigma_0(w',m)\, dw' \tag{14}$$

Charged tracks were selected requiring their point of closest approach to the beam axis be within 1 cm of the beam line, and their angle with respect to the beam axis, θ, to satisfy $|\cos\theta| < 0.93$ [22]. Photon candidates must have at least 25 (50) MeV of energy in the barrel (end cap) electromagnetic calorimeter (EMC) and have $|\cos\theta| < 0.82$ ($0.86 < |\cos\theta| < 0.92$).

The $e^+e^- \to \gamma\gamma$ events were selected using the following criteria

1. $N_q = 0$ and $N_\gamma > 1$, where N_q is the number of charged tracks and N_γ is the number of photons;
2. $|\cos\theta_i| < 0.8$, where here and below $i = 1,2$ denotes the photons with the highest energy deposition;
3. $|\Delta\theta| = |\pi - (\theta_1 + \theta_2)| < 0.05$;
4. $-0.06 < \Delta\phi < 0.02$, $\Delta\phi = \pi - |\phi_1 - \phi_2|$, where ϕ is the azimuthal angle around the beam direction;
5. $0.8 < E_i/E_{beam} < 1.2$, where E_i is the energy deposition in the EMC of the ith photon and E_{beam} is the beam energy.

In order to select multihadronic events the following criteria were applied.

1. $N_q > 3$;
2. $S > 0.06$, where $S = \frac{3}{2}(\lambda_2 + \lambda_3)$ is the sphericity parameter. Here $\lambda_1 \geq \lambda_2 \geq \lambda_3$ are eigenvalues of sphericity tensor:

$$S^{ij} = \frac{\sum N_{q_{n=1}} p_n^i p_n^j}{\sum_{n=1}^{N_q} p_n^2}$$

where p_i the momentum of the ith track.

The number of selected multihadronic events N^{mhad} were fitted by minimizing the likelihood function:

$$\chi^2 = \sum_{i=1}^{N} \frac{(N_i^{mhad} - \sigma^{mhad} L_i)^2}{N_i^{mhad}(1 + N_i^{mhad}/N_i^{ee,\gamma\gamma})} + \sum_{i=1}^{N} \left(\frac{w_i - W_i}{\Delta W_i}\right)^2. \tag{15}$$

The free parameters of the fit were ψ' mass m, σ_{bg}, ε, σ_w. The center of mass energy w_i at each energy point was fitted to the values W_i obtained as follows:

$$W = 2\sqrt{\varepsilon_{sip}^- \varepsilon_{sip}^+}\cos\frac{\alpha}{2} \tag{16}$$

where ε_{sip}^- and ε_{sip}^+ are the energies of the electron and positron beams, respectively, in the south interaction region calculated according to formula (11), $\alpha = 22$ mrad is the crossing angle of the beams. The error ΔW of the W determination is calculated from the errors of ε_{sip}^- and ε_{sip}^+.

The results of the fits for the two scans are in agreement. The results of the fit to all data are presented in Table 1 and in Fig. 21.

In order to check the adequacy of the selection criteria for multihadron events, even more strict cuts were applied for their selection:

- $N_q > 4$
- $p_t > 50$ MeV and $|\cos\theta| < 0.8$ for each charged track. Here p_t is the transverse momentum.

The fit was performed with the new number of selected multihadronic events, and $\Delta m = -17 \pm 58$ keV and $\sigma_w = 1.56 \pm 0.03$ MeV were obtained.

The luminosity determination was also tested using events of $e^+e^- \to e^+e^-$, scattered at small angles to suppress the contribution from $\psi' \to e^+e^-$ decay. The mass difference and beam energy spread were found to be $\Delta m = 17 \pm 50$ keV and $\sigma_w = 1.59 \pm 0.03$ MeV.

The bias of the center of mass energy obtained using the BEMS from the true value can be estimated as $\Delta m = m - m_{\psi'}$:

$$\Delta m = 1 \pm 56 \pm 24 \pm 40 \simeq 1 \pm 72\ \text{keV}. \tag{17}$$

Here the first error is the statistical, the second is due to systematical uncertainties of the luminosity determination and multihadronic event selection, and the last one is the error of the PDG $m_{\psi'}$ value. If we take the deviation of the measured beam

Table 1
The results of the fit. $\Delta m = m - m_{\psi'}$.

Δm (keV)	1 ± 56
σ_w (MeV)	1.58 ± 0.03
σ_{bg} (nb)	4.7 ± 0.1
ε (%)	32.7 ± 0.5
χ^2/ndf	13.5/8
$P(\chi^2,ndf)$(%)	9.7

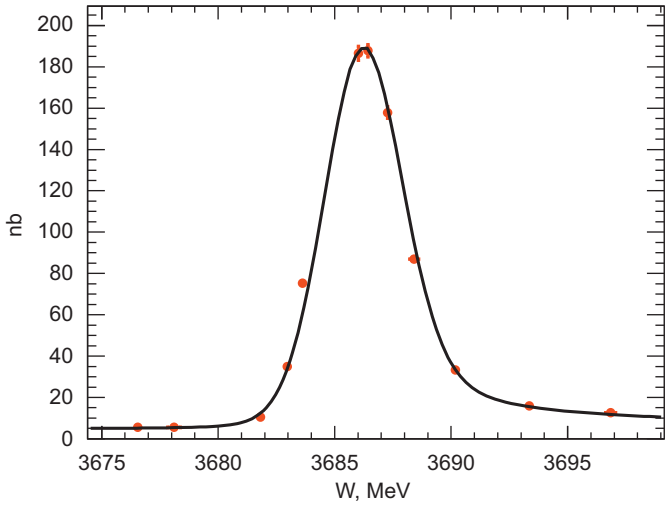

Fig. 21. Fit of the ψ'.

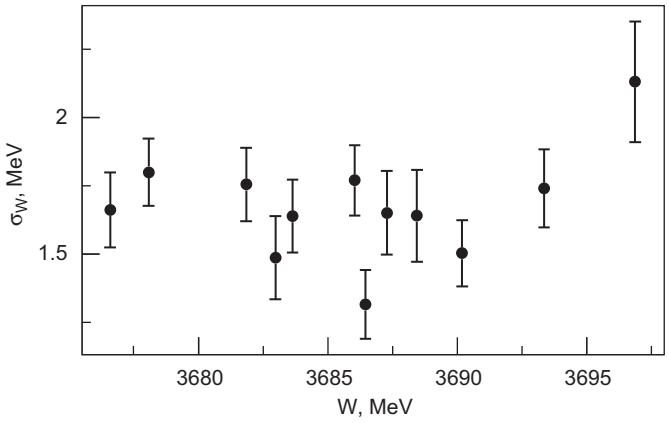

Fig. 22. The center-of-mass energy spreads obtained by means of the BEMS.

energy ΔE from the actual value as $\Delta\varepsilon = \Delta m/2$, then

$$\Delta\varepsilon = 1 \pm 36 \text{ keV} \tag{18}$$

Taking into account this deviation, the relative accuracy of the beam energy determination can be estimated as 2×10^{-5}.

The center-of-mass energy spreads σ_W obtained by using the BEMS at the 12 energies are shown in Fig. 22. The relative statistical accuracy of the σ_W determination per measurement is about 10%. The average of all measurements is $\sigma_W = 1.65 \pm 0.04$. The energy spread obtained from the fit of ψ' resonance is $\sigma_w = 1.58 \pm 0.03$. The difference between these two values $\sigma_W - \sigma_w = 0.07 \pm 0.05$ is about 1.4 standard deviations and consistent with zero. Using this difference, the relative systematical accuracy of the energy spread determination can be estimated as 6%.

7. Conclusion

The energy measurement system of the BEPC-II collider beams based on the Compton back-scattering method was designed, constructed, and put into operation. The systematical error of the beam energy determination is tested through measurement of the ψ' mass and is estimated as 2×10^{-5}.

Acknowledgment

The authors are grateful to A.E. Bondar, E.B. Levichev, Yu.A. Tikhonov for initiating and supporting the work. The work was supported in part by SB RAS joint project No. 32 for fundamental research with CAS; National Natural Science Foundation of China (10775412, 10825524, 10935008), Instrument Developing Project of Chinese Academy of Sciences (YZ200713), Major State Basic Research Development Program (2009CB825200, 2009CB825203, 2009CB825206) and Knowledge Innovation Project of Chinese Academy of Sciences (KJCX2-YW-N29); and by the Department of Energy under Contract No. DE-FG02-04ER41291 (University of Hwasii).

References

[1] J.Q. Wang, et al., Proceedings of IPAC'10, Kyoto, Japan, 2010, 2359.
[2] M. Ablikim, et al., Nuclear Instrumentation and Methods A 614 (2010) 345.
[3] D.M. Asner, et al., arXiv:0809.1869.
[4] K. Nakamura, et al., Particle Data Group, Journal of Physics G 37 (2010) 075021.
[5] Y.K. Wang, X.H. Mo, C.Z. Yuan, J.P. Liu, Nuclear Instrumentation and Methods A 583 (2007) 479.
[6] X.H. Mo, in: Proceedings of Ninth International Workshop on tau Lepton Physics, Pisa, Italy, September 19–22, 2006, Nuclear Physics Proceedings Supplement, vol. 169, 2007, p. 132.
[7] A.N. Skrinsky, Yu.M. Shatunov, Soviet Physics–Uspekhi 32 (1989) 548.
[8] J.Z. Bai, et al., Physics Review D 53 (1996) 20.
[9] T. Yamazaki, et al., IEEE Transactions on Nuclear Science NS-32 (5) (1985) 3406.
[10] I.C. Hsu, et al., Nuclear Instrumentation and Methods A 384 (1997) 307;
I.C. Hsu, et al., Physics Review E 54 (1996) 5657.
[11] R. Klein, et al., Nuclear Instrumentation and Methods A 384 (1997) 293;
R. Klein, et al., Journal of Synchrotron Radiation 5 (1998) 392;
R. Klein, et al., Nuclear Instrumentation and Methods A 486 (2002) 545.
[12] N. Muchnoi, et al., in: Proceedings of the EPAC, Scotland, Eidenburgh, June 26–30, 2006, EPAC 1181;
V.E. Blinov, et al., in: Proceedings of International Conference on Instrumentation for Colliding Beam Physics, Novosibirsk, Russia February 28–March 5, 2008, Nuclear Instrumentation and Methods A, vol. 598, 2009, p. 23;
V.E. Blinov, et al., ICFA Beam Dynamics Newsletters 48 (2009) 195;
O.V. Anchugov, et al., Zhurnal Eksperimentalaposnoi Teoreticka Fiziki 136 (2009) (Journal of Experimental and Theoretical Physics 109 (2009) 590).
[13] M.N. Achasov, et al., BINP Preprint 2008-4, ArXiv:0804.0159, 2008.
[14] M.N. Achasov, et al., in: Proceedings of the 10th International Workshop on Tau Lepton Physics, Novosibirsk, Russia, September 22–25, 2008, Nuclear Physics Proceeding Supplement, vol. 189, 2009, p. 366;
MO Xiao-Hu, et al., in: Proceedings of the International Workshop on e^+e^- Collisions from ϕ to ψ, October 13–16, 2009, Beijing, China, China Physics C, vol. 34(6), 2010, p. 912.
[15] C.K.N. Patel, Physics Review 136 (5A) (1964) 1187.
[16] E.V. Abakumova, et al., Vacuum Technic and Technology 20 (2) (2010) 77 (in Russian).
[17] P.F.A. Alkemade, C. Alderliesten, P. De Wit, C. Van der Leun, Nuclear Instrumentation and Methods A 197 (2–3) (1982) 383.
[18] Tibor Papp, X-Ray Spectrometry 32(6) (2003) 1097.
[19] M.C. Lee, K. verghese, R.P. Gardner, Nuclear Instrumentation and Methods A 262 (1987) 430.
[20] H. Siegert, H. Janssen, Nuclear Instrumentation and Methods A 286 (1990) 415.
[21] K. Yu. Todyshev, The application Breit–Wigner Form with Radiative Corrections to the Resonance Fitting, 〈http://arxiv.org/pdf/0902.4100v3〉.
[22] M. Ablikim, et al., Physics Review D 81 (2010) 052005.